Air entrainment by inclined circular plunging water jets with various impingement heights

Yiyi Ma, Luchen Zhang, Yu Yang and Ping Wei

ABSTRACT

This paper presents an experimental study on air entrainment by inclined circular plunging water jets issued from long nozzles with various jet impingement heights up to 6.1 m. Particular attention was paid to the jets having a large impingement height, and which disintegrated into small droplets before reaching the water surface. The dominant sizes and velocities of the droplets generated by jet breakup were 1–4 mm and 4–9 m/s. The results show that for plunging water jets having the same hydraulic head, the air entrainment rate increased as the jet impingement height at first grew, then dropped as the jet impingement height kept increasing. The early increase in the air entrainment rate was due to the growth of jet surface roughness, while the later decrease was caused by the water jet disintegration. The momentum of the plunging jet decreased dramatically due to the reduced mass and the significant energy dissipation through the atmosphere caused by jet disintegration. This led to a much smaller penetration depth and air entrainment rate compared to with a continuous jet.

Key words | air entrainment, bubble, inclined plunging water jet, jet impingement height, water droplet, water jet breakup

Yiyi Ma
Department of Civil Engineering,
Zhejiang University,
Hangzhou 310058,
China

Luchen Zhang
Yu Yang (corresponding author)
Ping Wei
MWR Nanjing Hydraulic Research Institute,
Nanjing 210029,
China
E-mail: *yyang@nhri.cn*

HIGHLIGHTS

- Air entrainment by plunging water jets with various impingement heights was presented.
- The appearance of plunging jets with various impingement heights at water surface was presented.
- The bubbly flows generated by jets with different impingement heights were compared.
- The variation of air entrainment rate was studied under a wide range of jet impingement heights.
- The jet impingement height corresponding to the maximum air entrainment rate by plunging jets with the same hydraulic head was discussed.

INTRODUCTION

Air entrainment by the impact of falling jets on a liquid surface is common in nature and also widely observed in engineering processes, such as in dam spillway flow and the wastewater treatment industry (Hammad 2010; Qu *et al.* 2011; Qu *et al.* 2013; Harby *et al.* 2014).

Previous studies have investigated the generation of air bubbles by plunging water jets, like EI Hummoumi *et al.* (2002), Chanson *et al.* (2004) and Roy *et al.* (2013), etc. Air entrainment is triggered when the jet impact velocity exceeds the inception velocity (EI Hummoumi *et al.* 2002; Chanson *et al.* 2004). An air envelope is formed surrounding the impingement perimeter of the plunging liquid jet, which is then elongated and deforms as the plunging jet penetrates the water (Mckeogh & Ervine 1981; EI Hummoumi *et al.* 2002). The air envelope eventually disintegrates into small bubbles due to shear stress, and thus generates a bubbly flow below the water surface (Chanson *et al.* (2004), Roy *et al.* 2013). The features of air entrainment by plunging

doi: 10.2166/ws.2020.246

water jets have been studied extensively, regarding the flow field beneath the water surface, the entrained bubbles, and the air entrainment rate, etc. Kusabiraki *et al.* (1990), Hammad (2010) and Harby *et al.* (2014) reported the velocity variation in the bubbly flow for vertically plunging water jets. They also found that the penetration depth of plunging jets is affected by the nozzle diameter and length, jet exit velocity and jet impingement height. In their experiments, Chanson *et al.* (2004) found that the size distribution of the entrained bubbles is related to the jet impact velocity.

The entrained air flow rate typically depends on the parameters of the air/fluid properties (density, surface tension, viscosity, etc.) and flow conditions (jet velocity, size, impingement height, angle, etc.), as summarized in Miwa *et al.* (2019). Essentially, the jet surface roughness plays an important role in the air entrainment of a plunging jet (Van de Sande & Smith 1973, Ervine *et al.* (1980), Kusabiraki *et al.* 1990; Oguz 1998). Ervine *et al.* (1980) and Kusabiraki *et al.* (1990) both obtained a greater air entrainment rate when increasing the jet impingement height. A large impingement height caused a significant growth of the jet surface roughness, thereby resulting in a high air entrainment rate.

Although a considerable number of studies have been reported for air entrainment of plunging liquid jets, most of them were conducted with a limited impingement height (h), e.g., $h = 0.02$ m in Lin & Donnelly (1966), up to $h = 1.05$ m in Ahmed (1974), $h = 0.2$ m in Van de Donk (1981), up to $h = 0.75$ m in Kusabiraki *et al.* (1990), up to $h = 0.3$ m in Chanson & Manasseh (2003), and $h = 0.4$ m in Deshpande *et al.* (2012), where the plunging water jets were kept continuous before impacting on the water surface. Few studies have been conducted with a jet impingement height larger than 500 times the nozzle exit diameter, as summarized by Miwa *et al.* (2019). However, with a large jet impingement height, a falling water jet can disintegrate into small droplets under the aerodynamic effects (Sallam *et al.* 2002; Pan & Suga 2006; Ma *et al.* 2016), which results in quite different features of air entrainment compared to continuous water jets. Also, in the previous studies, the variation of air entrainment was commonly discussed within a limited range of jet impingement height, where cases of disintegrated jets were seldom included.

The present study reports the experimental investigation of the air entrainment of an inclined circular plunging water jet with various impingement heights up to 6.1 m, and a ratio of the impingement height to the nozzle exit diameter h/D_0 of up to 760. Images of the falling water jet before impacting on the water surface and the bubbly flow below the water surface were captured with a high-speed camera. The features of the bubbly flow, including the penetration depths, the bubble size distribution, bubble velocity and void fraction, were studied. The air entrainment rates of plunging jets with different impingement heights were measured and compared. The present study extends the range of jet impingement height for experimental study on air entrainment by plunging jets, and adds to the existing knowledge in this research area.

EXPERIMENTS

The experimental setup for studying the air entrainment of an inclined plunging water jet is shown in Figure 1(a). It was a closed-loop flow system and mainly consisted of a tank, a pump and a standpipe. The tank was 1 m × 3 m × 1 m, fabricated from transparent plexiglass for visualization. The tank was filled with water first and water was pumped from the tank to the standpipe through a horizontal inflow pipe. The standpipe had a total height of about 10 m and a diameter of 0.2 m. Nozzles were installed at various positions on the standpipe while the water elevation in the standpipe was kept for the desired jet hydraulic head. The water elevation in the standpipe was monitored with a pressure transducer (HQ1300 transducer, Huaqiang Inc., Baoji, China) and controlled by adjusting the valve in the horizontal inflow pipe. Long nozzles made of plexiglass were used in the experiments, with a length of $L = 0.92$ m and various diameters of $D_0 = 5$, 8, 10 and 15 mm. The length-to-diameter ratios of the nozzles were $L/D_0 = 61.3$–184 and fully developed turbulent flow could be formed at the nozzle exit. As $L/D_0 > 15$ in the current experiments, the effect of L/D_0 on the jet shape (the degree of the jet surface roughness) is imperceptible, based on Kusabiraki *et al.* (1990). The nozzles were installed at the positions of $h = 0.6$, 1.9, 3.0 and 6.1 m, which were also the jet impingement heights. In each test, the water flow rate was measured using the volume/time method.

The appearances of the falling jet before impacting on the water surface and the bubbly flow below the water surface were recorded with a high-speed camera (Phantom

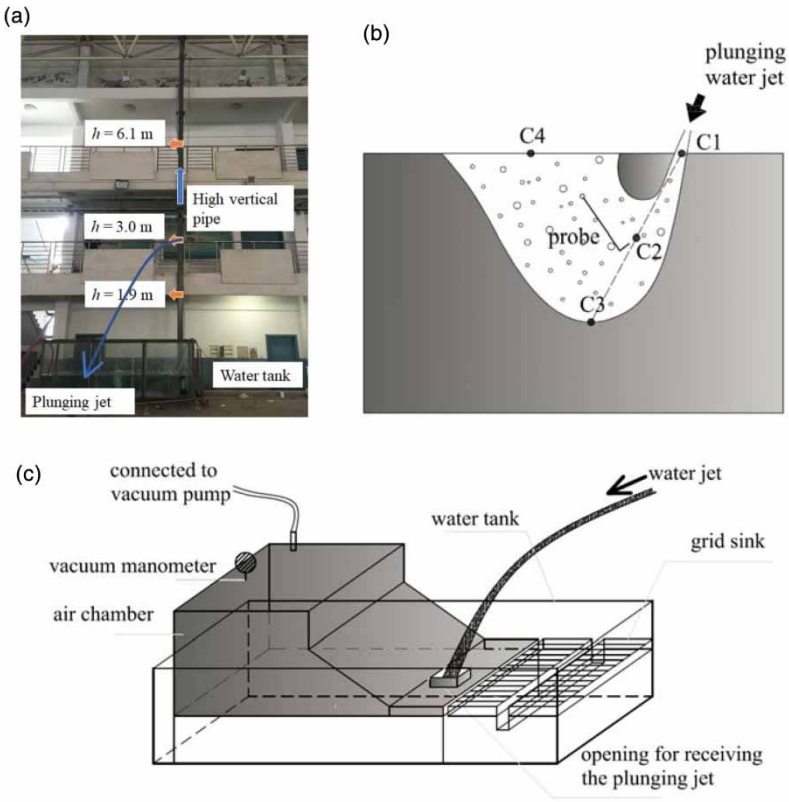

Figure 1 | (a) Photograph of the experimental setup; (b) measuring locations for RBI 1501 optical probe; (c) the air chamber for collecting the entrained air bubble.

V10, Vision Research, Wayne, New Jersey), at a speed of 480 frames per second and a resolution of $2{,}400 \times 1{,}800$ pixels. The backlight was adopted for photography, provided by a 600 mm × 600 mm array of high-power light-emitting diodes (LED). The entire bubble velocity distribution in the bubbly flow was obtained from the high-speed camera images by PIVlab (Thielicke 2014; Thielicke & Stamhuis 2014). A steel ruler with a precision of 1 mm was used for length scale calibration during image processing.

An RBI 1501 optical probe (RBI instrumentation, Meylan, France) was also utilized to measure the bubbly flow properties, including the void fraction, bubble size, bubble velocity, etc. The RBI 1501 optical probe comprised a probe, an optoelectronic unit, and an ISO lite acquisition unit. The probe had a tip of 40 μm diameter, a stability time of 0.5–1.0 μs and a maximum measurable velocity of 30 m/s. The acquired data were processed with the RBI ISO software. The measuring locations for the bubbly flow are labeled as C1-C4 in Figure 1(b). These locations were defined qualitatively: C1 was approximately at the center of the plunging point, C3 was the lowest position of the bubbly flow, C2 was in the middle of C1 and C3, while C4 was at the center of the bubbly flow released at the water surface. The sampling duration at each point was about 60 seconds and each measurement was repeated twice.

The amount of entrained air was measured by using an air chamber placed in the water tank, which mainly consisted of a chamber for air collection, a front plate and a grid sink for water level control, as illustrated in Figure 1(c). The top of the chamber was airtight while the bottom was completely open. A vacuum pump was installed at the top of the chamber together with a vacuum manometer. There was a square opening of 0.1 m × 0.1 m on the front plate for receiving the plunging water jet (Figure 1(c)). The grid sink was height adjustable and a pipe was installed on the bottom for overflow drainage. When the water level in the tank exceeded the grid sink elevation, water flowed into the sink and got drained out of the tank through the bottom pipe.

To measure the volume of entrained air, the water level in the tank was controlled to be flush with the front plate. At

the beginning of the experiments, the air was extracted out of the chamber by the vacuum pump, which caused the rise of the water level in the chamber. When the chamber was filled with water, the vacuum pump was stopped. In the experiments, air bubbles were introduced into the water by the plunging water jet through the opening on the front plate. The entrained air bubbles penetrated the water with the plunging jet, moved obliquely upward into the chamber and finally accumulated at the chamber top. Due to the air accumulation at the top, the water level in the chamber fell gradually. When the water level in the air chamber became the same as that in the water tank, the experiment was ended. At this moment, the reading of the vacuum manometer turned into 0, i.e., the air pressure inside the chamber was atmospheric pressure. The air entrainment rate of the plunging water jet could then be calculated by dividing the volume of the collected air in the chamber by time. Note that when having an impingement height of $h = 6.1$ m, the water jet spread so widely that it could not impact on the water surface within the opening on the front plate. This caused difficulties in collecting the entrained air and led to errors in measurement. Therefore, air volume measurement was not conducted for this scenario. The experiments in this study were conducted with tap water and ambient air at a room temperature of about 15 °C.

The uncertainties of the experiments mainly lay in the collection of entrained air, measurement of penetration depth, and droplet velocity/size acquisition by image processing. To be specific, the fact that a small portion of water occasionally impacted outside the opening due to turbulence when collecting the entrained air and the oscillation of the lowest position of bubbly flow both bring uncertainties to the experimental results. Uncertainties can also occur when transferring the droplet velocity and size from the image scale to their actual dimensions.

EXPERIMENTAL RESULTS AND DISCUSSION

Jet appearance before impacting on water surface

Images of the plunging water jets at different locations, i.e., about 30 cm above the water surface, at the water surface, and below the water surface, are presented in Figure 2, with jet impingement heights of $h = 0.6$ and 6.1 m, and nozzle diameters of $D_0 = 15$ and 8 mm. The field view of each image in Figure 2 is about 0.3 m × 0.33 m. It is seen that under a small impingement height of $h = 0.6$ m, the falling water jet stays continuous all the way to the plunging point. In this case, only a small number of splashes and relatively weak turbulence are observed at the plunging point (Figure 2(a)(I, II)). For the water jets with a large impingement height of $h = 6.1$ m, the majority of the jet has disintegrated into small droplets before impacting on the water surface, as shown in Figures 2(b)(I, II) and 2(c)(I, II).

In the current study, droplet diameter was defined as the diameter of the circle having the same area as the droplet detected from the images. For each test, droplet diameters were obtained with MATLAB image processing tools based on over 900 continuously-taken images. The droplet size distributions of the jets of $D_0 = 15$ and 8 mm, with a large impingement height of $h = 6.1$ m, are presented in Figure 3. Note that there were occasionally water 'ligaments' with a relatively large size captured in the images, of which the amount occupied less than 2% of the total numbers. These water ligaments were not included when analyzing the water droplet size distribution. Based on Figure 3, the falling water jets of $D_0 = 15$ and 8 mm both show dominant droplet diameters of $d_e = 1$–4 mm. The droplet velocities were obtained from the images by using PIVlab, as shown in Figure 4. It can be seen that water jets of $D_0 = 15$ and 8 mm both have a dominant droplet velocity of about $V =$ 8 m/s. Combining the results presented in Figures 3 and 4, the droplets released from the two falling water jets with the same impingement height but of different sizes exhibit similar features. Ferro (2001) developed an equation for the terminal velocity of raindrops in the air: $V_t = 9.5[1 - \exp(-0.6d_e)]$. Based on this equation, the terminal velocity of the droplets with a diameter of $d_e = 1$–4 mm is calculated to be $V_t = 4.3$–8.6 m/s, which is consistent with the results in Figure 4. This shows that the droplets resulting from the disintegration of the water jets discharged from $h = 6.1$ m fell at terminal velocity before impacting on the water surface. Additionally, unlike the plunging jet with a short impingement height, the impact of the droplets causes strong turbulence and a large number of splashes at the water surface, as shown in Figures 2(b)(II) and 2(c)(II).

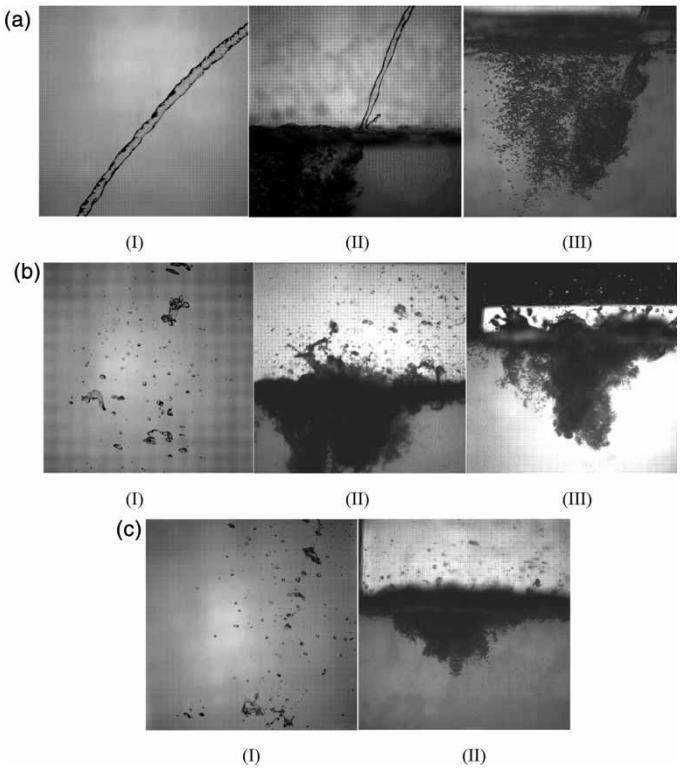

Figure 2 | The appearance of jets under different conditions: (a) $h = 0.6$ m, $D_0 = 15$ mm; (b) $h = 6.1$ m, $D_0 = 15$ mm; (c) $h = 6.1$ m, $D_0 = 8$ mm. The images labelled with (I), (II) and (III) represent the positions of 30 cm above the water surface, at the water surface and below the water surface, respectively.

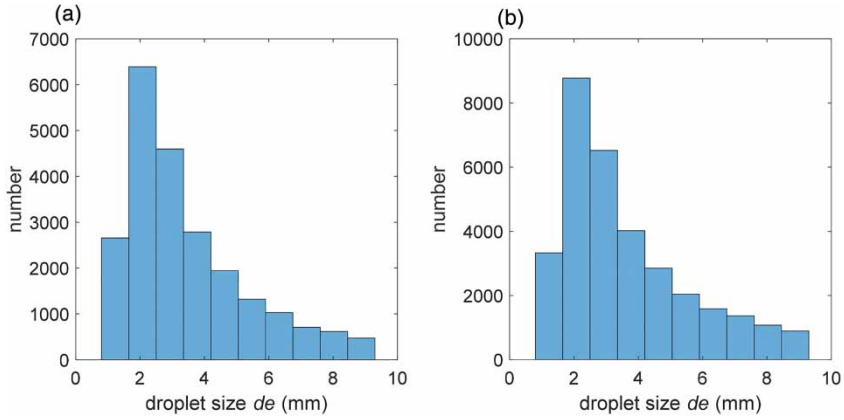

Figure 3 | Droplet size distribution of a falling water jet about 30 cm above of the water surface: (a) $D_0 = 15$ mm, $h = 6.1$ m; (b) $D_0 = 8$ mm, $h = 6.1$ m.

Bubbly flow features

The bubbly flows generated by the plunging water jets of $D_0 = 15$ and 8 mm with $h = 0.6$ m and 6.1 m are shown in Figures 2(a)(III), 2(b)(III) and 2(c)(II). The bubbles formed by the jets with an impingement height of $h = 6.1$ m are less dispersive than those formed by the jet with $h = 0.6$ m, which causes difficulty in analyzing the bubble features from the images. Thus, the bubble features are discussed only for those generated by the jet of $h = 0.6$ m with an exit velocity of $V_0 = 2.0$ m/s (Figure 2(a)(III)). The jet impact velocity of V_p can then

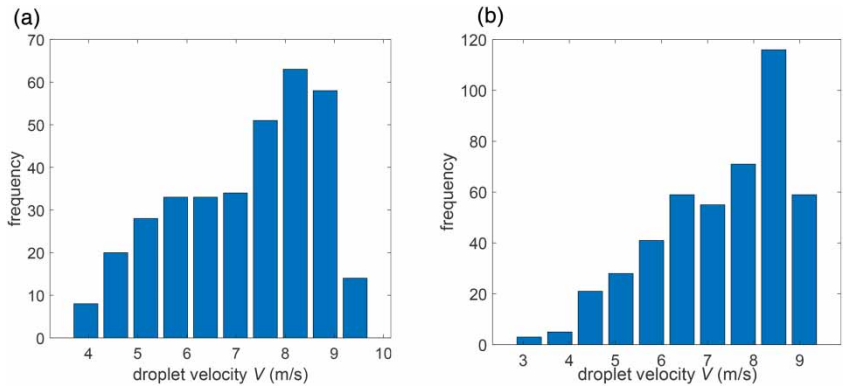

Figure 4 | Droplet velocity distribution of a falling water jet 30 cm above of the water surface: (a) $D_0 = 15$ mm, $h = 6.1$ m; (b) $D_0 = 8$ mm, $h = 6.1$ m.

be estimated as $V_p = (V_0^2 + 2\,gh)^{0.5} = 4.4$ m/s (Qu *et al.* 2013; Harby *et al.* 2014).

Based on the high-speed camera photography, the bubbly flow was found to mainly contain two parts: downward and upward bubble flows. It is understood that the bubbles are imposed on drag by the downward plunging jet and buoyancy force, which act in opposite directions. The relative strength of the two forces determines the moving direction of the bubbles. The bubbles move downward first, carried by the plunging water jet, with decreasing velocity with depth. At a certain position, the downward bubble velocity becomes zero, and then the bubbles start rising towards the water surface. The position of such a point is typically unsteady and oscillates. The distance from the water surface to this point is considered as the penetration depth of the plunging jet. The bubble size distribution is not even in the bubbly flow. As shown in Figure 2(a)(III), intermittent large air cavities are formed right below the impact position of the plunging jet. The large air cavity is then broken down into small bubbles by the turbulence and move downwards surrounding the plunging jet. The rising bubbles disperse in the shape of a cone and show relatively larger bubbles compared to the downward ones.

Figure 5 shows the average bubble velocity distribution obtained by PIVlab based on a total of 100 images. It is seen that the bubble velocity is much smaller than the jet impact velocity. Note that the bubble spatial distribution in the downward bubble flow is not as dispersive as the upward flow, which causes difficulty in detecting the bubble velocity from the images. Thus, uncertainties can occur in the measurement of downward bubble velocity by PIVlab. The void fraction of bubbly flow, frequency, bubble velocity and size, were also measured with the RBI 1501 optical probe at C1-C4, as presented in Table 1. The

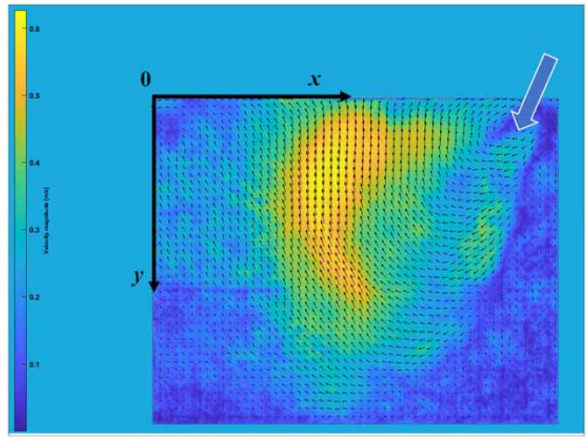

Figure 5 | Averaged bubble velocity distribution in the bubbly flow generated by an inclined plunging water jet of $D_0 = 15$ mm and $h = 0.6$ m with an exit velocity of $V_0 = 2.0$ m/s.

Table 1 | Bubble characteristics measured by the RBI 1501 optical probe at C1-C4 ($h = 0.6$ m, $D_0 = 15$ mm)

Measurement position	Void fraction α (%)	Frequency (Hz)	Bubble velocity (m/s)	Averaged Sauter mean diameter (mm)
C1	44.6	282.0	4.6	10.8
C2	27.0	666.2	3.6	2.2
C3	9.6	30.1	0.7	3.5
C4	3.6	7.2	0.4	3.1

void fraction (i.e., the proportion of time for the probe tip inside the air bubble) is maximum near the jet plunging position, which reaches 44.6%, while it decays gradually along the jet penetrating path and reduces to 9.6% at the lowest position of the bubbly flow. When the bubbles move upwards to the water surface, the void fraction decreases to 3.6%. The variation of void fraction in bubbly flow is consistent with the spatial density of bubbles observed from the images (see Figure 2(a)(III)), which verifies the reliability of the probe. The bubble velocity is close to the jet plunging velocity near the impact point and keeps decreasing from C1 to C3. The bubble rising velocity near the water surface is small, only 0.4–0.5 m/s based on the probe measurements, which agrees with the PIVlab analysis. From Table 1, a large bubble size is found at C1, which is due to the air cavity formed near the jet plunging point. From C1 to C2, the bubble size is reduced significantly. The plunging water jet still remains at high velocity and the strong air-water interaction in this region breaks up the entrained air bubbles into ones of small size. From C2 to C3, due to the significant decay of water velocity, the bubbles slow down and coalesce, leading to an increase in the bubble size. For the air bubbles traveling upwards from C3 to C4, where the kinetic energy of the plunging water jet has been mostly dissipated and the turbulence is weak, no significant change in bubble size is observed.

The penetration depths of the plunging water jets of various sizes with impingement heights of $h = 2.8$ m and $h = 6.1$ m are listed in Table 2, when the hydraulic heads of the jet (i.e., the water depth in the standpipe) are $H = 6.5$ m and 9.0 m. The results show that with the same jet size and the same impingement height of $h = 2.8$ m, the penetration depth increases by 20% on average when the jet hydraulic head increases from $H = 6.5$ m to 9.0 m. This is due to the higher jet exit velocity after raising the jet hydraulic head. Additionally, with the same jet hydraulic head of $H = 6.5$ m and the same impingement height of $h = 2.8$ m (i.e., the same jet exit velocity), the penetration depth increases with the jet size. A larger jet size corresponds to an increased mass and thus more considerable momentum of the plunging jet, which is the reason for the larger penetration depth. However, when the impingement height is increased to $h = 6.1$ m while the jet hydraulic head remains $H = 6.5$ m, the penetration depth is significantly reduced to 0.15 m and 0.06 m for water jets of $D_0 = 15$ and 8 mm. The reason for this reduction is explained in the following. Under an impingement height of 6.1 m, the falling water jet has disintegrated into small droplets before reaching the water surface. The droplets fall in the terminal velocity through the atmosphere and suffer considerable energy dissipation. The reduced mass of individual droplets compared to a continuous jet, as well as the energy dissipation through the atmosphere, lead to a dramatic decrease in the momentum of the plunging jet and thereby result in a smaller penetration depth.

Table 2 | Penetration depth (m) of the plunging water jets under different conditions

	$H = 6.5$ m		$H = 9.0$ m
Nozzle size (mm)	$h = 2.8$ m	$h = 6.1$ m	$h = 2.8$ m
5	0.16	/	0.19
8	0.22	0.06	0.26
10	0.27	/	0.34
15	0.34	0.15	0.40

Air entrainment rate

The following discussion is conducted for water jets having the same hydraulic head of $H = 6.1$ m. The air entrainment rates of plunging water jets under different experimental conditions are shown in Figure 6. Figure 6(a) presents the air entrainment rates of the plunging jets of various sizes discharged from $h = 0.6$ m and 3.0 m. It can be seen that with the same jet impingement height (i.e., the same jet exit velocity), the air entrainment rate of the plunging jet increases with the jet diameter. In Figure 6(b), for the plunging jet with $D_0 = 10$ mm under two impingement heights of $h = 3.0$ m and 1.9 m, the air entrainment rate approximately increases linearly with the jet exit velocity. Figure 6(c) shows the variation of air entrainment rate with impingement height for the jets of $D_0 = 10$ and 15 mm. Theoretically, without air resistance and jet disintegration, the jet impact velocity is only dependent on the jet hydraulic head and free from the influence of jet impingement height. Under such an ideal condition, the air entrainment rate with different jet impingement heights should be the same. However, as observed from the experiments, the air entrainment

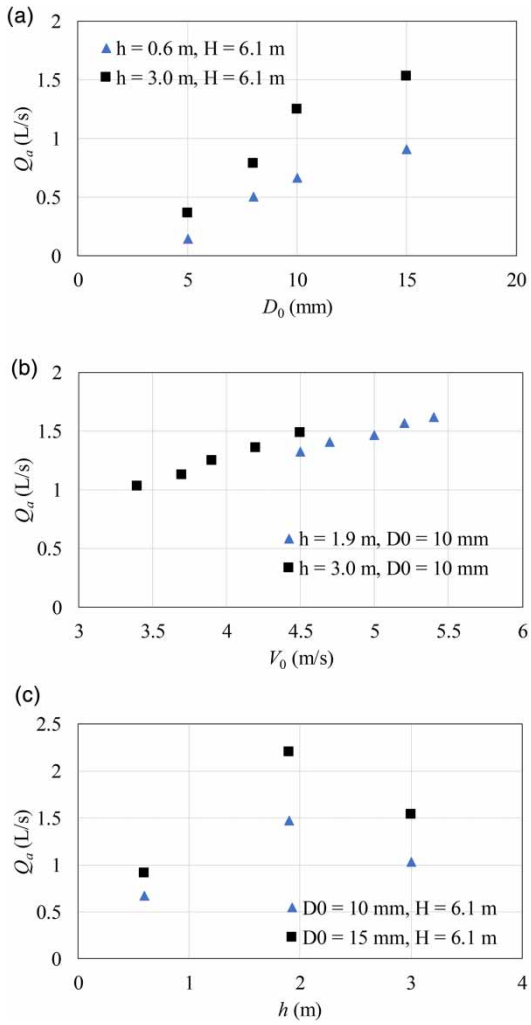

Figure 6 | Variation of air entrainment rate of inclined plunging water jets with (a) jet size; (b) jet exit velocity ($D_0 = 10$ mm) and (c) jet impingement height. All the data were obtained with a jet hydraulic head of $H = 6.1$ m.

rate increases when the impingement height increases from $h = 0.6$ m to 1.9 m, whereas it drops as the impingement height further increases to $h = 3$ m. Air resistance plays an important role in this variation. The increase of the air entrainment rate from $h = 0.6$ m to 1.9 m is due to the growth of the jet surface roughness under the effect of air resistance, as reported in Ervine *et al.* (1980), Kusabiraki *et al.* (1990) and Harby *et al.* (2014). However, when the impingement height further increases, the falling water jets disintegrate into small droplets due to the air-water interaction. These droplets reach terminal velocity after a certain falling distance and much energy is dissipated. This leads to a decrease in the momentum and, consequently, a reduced penetration depth as discussed in the previous section. This is the reason for the later reduction of the air entrainment rate in Figure 6(c).

The current study presents a detailed view of air entrainment by disintegrated water jets with a large impingement height and a comparison to continuous jets, which adds to the existing knowledge in this research area. Based on the variation of air entrainment rate with jet impingement height in the current experiments, there can be an impingement height corresponding to the maximum air entrainment rate, which can be considered when designing aeration devices.

CONCLUSIONS

This paper presented an experimental study of air entrainment by inclined plunging water jets with various impingement heights, with particular attention paid to the plunging jets with large impingement heights up to 6.1 m. The experimental results showed that a water jet having a small impingement height remained continuous while one with an impingement height of 6.1 m disintegrated into small droplets before impacting on the water surface. The droplets resulting from the jet breakup showed a dominant size of 1–4 mm and a terminal velocity of about 8 m/s. The penetration depth of the plunging jet with a large impingement height of 6.1 m was significantly reduced compared to that with a small impingement height. The disintegration of the jet into droplets caused a decrease in mass and considerable energy dissipation through the atmosphere, leading to a dramatic reduction in the momentum of the plunging jet. Thus, the disintegrated jets showed a smaller penetration depth and a lower air entrainment rate than continuous jets with a relatively short impingement height.

Based on the experimental results obtained under a wide range of jet impingement heights, the air entrainment rate first increased with the jet impingement height and then decreased as the jet impingement height kept increasing. The first increase of air entrainment rate was caused by the significant growth of the jet surface roughness while the later reduction was due to the jet disintegration. Thus, there can be a certain impingement height corresponding

to the maximum air entrainment rate, which can be taken into consideration when designing aeration devices.

ACKNOWLEDGEMENTS

The authors gratefully acknowledge financial support from the National Natural Science Foundation of China (Grant No. 51579150).

DATA AVAILABILITY STATEMENT

All relevant data are included in the paper or its Supplementary Information.

REFERENCES

Ahmed, A. 1974 *Aeration by Plunging Liquid Jet.* PhD Thesis, Loughborough University of Technol., UK.

Chanson, H., Aoki, S. I. & Hoque, A. 2004 Physical modelling and similitude of air bubble entrainment at vertical circular plunging jets. *Chemical Engineering Science* **59** (4), 747–758.

Chanson, H. & Manasseh, R. 2003 Air entrainment processes in a circular plunging jet: Void-fraction and acoustic measurements. *Journal of Fluids Engineering* **125** (5), 910–921.

Deshpande, S., Trujillo, M., Wu, X. & Chahine, G. 2012 Computational and experimental characterization of a liquid jet plunging into a quiescent pool at shallow inclination. *International Journal of Heat and Fluid Flow* **34**, 1–14.

El Hummoumi, M., Achard, J. L. & Davoust, L. 2002 Measurements of air entrainment by vertical plunging liquid jets. *Experiments in Fluids* **32**, 624–638.

Ervine, D. A., McKeogh, E. & Elsawy, E. M. 1980 Effect of turbulence intensity on the rate of air entrainment by plunging water jets. *Proceedings of the Institution of Civil Engineers* **69** (2), 425–445.

Ferro, V. 2001 Measurement and monitoring techniques of soil erosion processes. *Quad. Idron. Mont.* **21** (2), 63–128.

Hammad, K. J. 2010 Liquid jet impingement on a free liquid surface: PIV study of the turbulent bubbly two-phase flow. In: *ASME 2010 3rd Joint US-European Fluids Engineering Summer Meeting Collocated with 8th International Conference on Nanochannels, Microchannels, and Minichannels*. American Society of Mechanical Engineers Digital Collection, pp. 2877–2885.

Harby, K., Chiva, S. & Muñoz-Cobo, J. L. 2014 An experimental study on bubble entrainment and flow characteristics of vertical plunging water jets. *Experimental Thermal and Fluid Science* **57**, 207–220.

Kusabiraki, D., Niki, H., Yamagiwa, K. & Ohkawa, A. 1990 Gas entrainment rate and flow pattern of vertical plunging liquid jets. *The Canadian Journal of Chemical Engineering* **68** (6), 893–903.

Lin, T. J. & Donnelly, H. G. 1966 Gas bubble entrainment by plunging laminar liquid jets. *AIChE Journal* **12** (3), 563–571.

Ma, Y., Zhu, Z., Rajaratnam, N. & Camino, A. 2016 Experimental study of the breakup of a free-falling turbulent water jet in air. *Journal of Hydraulic Engineering* **142** (10), 06016014.

McKeogh, E. J. & Ervine, D. A. 1981 Air entrainment rate and diffusion pattern of plunging liquid jets. *Chemical Engineering Science* **36** (7), 1161–1172.

Miwa, S., Xiao, Y. G., Saito, Y. & Hibiki, T. 2019 Experimental study of air entrainment rates due to inclined liquid jets. *Chemical Engineering & Technology* **42** (5), 1059–1069.

Oguz, H. 1998 The role of surface disturbances in the entrainment of bubbles by a liquid jet. *Journal of Fluid Mechanics* **372**, 189–212.

Pan, Y. & Suga, K. 2006 A numerical study on the breakup process of laminar liquid jets into a gas. *Physics of Fluids* **18** (5), 052101.

Qu, X. L., Khezzar, L., Danciu, D., Labois, M. & Lakehal, D. 2011 Characterization of plunging liquid jets: a combined experimental and numerical investigation. *International Journal of Multiphase Flow* **37** (7), 722–731.

Qu, X., Goharzadeh, A., Khezzar, L. & Molki, A. 2013 Experimental characterization of air-entrainment in a plunging jet. *Experimental Thermal and Fluid Science* **44**, 51–61.

Roy, A. K., Maiti, B. & Das, P. K. 2013 Visualisation of air entrainment by a plunging jet. *Procedia Engineering* **56**, 468–473.

Sallam, K. A., Dai, Z. & Faeth, G. M. 2002 Liquid breakup at the surface of turbulent round liquid jets in still gases. *International Journal of Multiphase Flow* **28** (3), 427–449.

Thielicke, W. 2014 *The Flapping Flight of Birds: Analysis and Application*. PhD Thesis, University of Groningen.

Thielicke, W. & Stamhuis, E. 2014 PIVlab–towards user-friendly, affordable and accurate digital particle image velocimetry in MATLAB. *Journal of Open Research Software* **2** (1), e30. DOI: http://doi.org/10.5334/jors.bl.

Van de Donk, J. 1981 *Water Aeration with Plunging Jets*. PhD Thesis, TH Delft, The Netherlands.

Van de Sande, E. & Smith, J. M. 1973 Surface entrainment of air by high velocity water jets. *Chemical Engineering Science* **28** (5), 1161–1168.

First received 6 March 2020; accepted in revised form 20 September 2020. Available online 5 October 2020